Scientific Research Publishing

Open Journal of Fluid Dynamics, 2022, 12, 96-126
https://www.scirp.org/journal/ojfd
ISSN Online: 2165-3860
ISSN Print: 2165-3852

Experimental Study of the Diffusion of a Confined Wall Jet through a Perforated Plate: Influence of the Porosity and the Geometry

Moussa Diop[1*], Denis Flick[2], Graciela Alvarez[1], Jean Moureh[1]

[1]Refrigerating Process Engineering Unit, INRAE Antony, Antony, France
[2]UMR SayFood, AgroParisTech, INRAE, Université Paris Saclay, Massy, France
Email: *moussa.diop@outlook.com

How to cite this paper: Diop, M., Flick, D., Alvarez, G. and Moureh, J. (2022) Experimental Study of the Diffusion of a Confined Wall Jet through a Perforated Plate: Influence of the Porosity and the Geometry. *Open Journal of Fluid Dynamics*, **12**, 96-126.
https://doi.org/10.4236/ojfd.2022.121006

Received: December 20, 2021
Accepted: March 22, 2022
Published: March 25, 2022

Abstract

This paper investigated lateral diffusion of a confined two-dimensional wall jet (air inlet height: 5 cm) through a perforated plate. We considered two plates with porosities of $\phi = 0.3$ and $\phi = 0.5$. The plates were positioned at distances of 10 cm and 20 cm below the jet inlet. The experiments were realized using 2D Laser Doppler Anemometer (LDA). Different profiles of mean and fluctuating velocities are presented. The presence of a perforated plate strongly modified the airflow pattern compared to an empty enclosure. The velocities above and below the plate depend on several parameters, including the porosity and the plate's position relative to the inlet slot and the longitudinal position. The difference between the flow velocity above and below the plates could not be related using a universal formula that depends on these parameters. We also investigated the influence of a porous media of a height of 20 cm (a stack of spheres having a diameter of 3.75 cm) located below the perforated plate. The results highlight that the porous medium strengthens the effects of the perforated plate on the flow.

Keywords

Porous Medium, Perforated Plate, Wall Jet, Air Ventilation, Aeraulic, Turbulence Diffusion

1. Introduction

Most investigations involving a perforated plate focus on the evaluation of the pressure deficit through a perforated plate placed perpendicularly to the flow direction [1]-[7]. Some investigations in which the perforated plate/porous me-

dium is tangential to a flow may concern Stokes flow [8] [9], the results of which are not applicable in the case of high Reynolds number flows. These investigations focus on the interface conditions between the perforated plate/porous medium and the clear flow. In fact, Beavers and Joseph [9] were the first to investigate the flow over a porous medium. They investigated a Poiseuille flow experimentally over a naturally permeable bed. Their results highlighted the existence of a velocity discontinuity at the interface between the two media through the following relation:

$$\frac{\mathrm{d}u}{\mathrm{d}z} = \frac{\alpha}{\sqrt{K}}\left(u_s - u_D\right) \tag{1}$$

where u_s is called "slip velocity", u_D is the Darcian velocity in the porous medium, and α is a dimensionless coefficient called slip coefficient.

This relation arises from the existence of two media where two different equations govern the flow. The Stokes equations govern the clear region:

$$-\frac{\mathrm{d}p}{\mathrm{d}x} + \mu\frac{\mathrm{d}^2u}{\mathrm{d}z^2} = 0 \tag{2}$$

In this relation, z is the coordinate for the wall-normal direction, and x is the coordinate for the longitudinal direction.

In the porous media, the empirical Darcy law governs the flow:

$$-\frac{\mu}{K}u_D = \frac{\mathrm{d}\prec p\succ_v^f}{\mathrm{d}x} \tag{3}$$

where μ is the fluid's viscosity, K is the permeability of the porous medium, $\prec p\succ_v^f$ is the fluid phase-averaged pressure, and u_D is the Darcian velocity. u_D is the volume-averaged velocity of a local elementary volume located away from the interface. The volume average for the velocity is taken over the fluid and solid phases:

$$u_D = u_v\left(z \to -\infty\right) \tag{4}$$

Since the Darcian velocity is considered in the porous region instead of the local velocity, a velocity discontinuity arises at the interface of the two media. A mathematical justification of the interface condition Equation (1) was derived by Saffman [10].

Several other investigations of the flow over a porous medium attempting to account for the slip velocity have been carried out [9] [11] [12] [13] [14]. Moreover, several other methods have been proposed, including the Brinkman interface condition accounting for the slip velocity through an "effective" viscosity $\tilde{\mu}$ and the interface condition of Brinkman [15]-[28]. The result of these investigations is the impossibility of deducing an analytical formula that describes the interface conditions.

A similar situation concerning the conditions at the interface between a clear flow and a perforated plate has also been observed on flows over a perforated plate. For example, Laplace and Arquis [8] showed that the flow at the interface perforated plate/clear flow is governed by the following relation relating the ve-

locity gradient to the slip condition:

$$\frac{\mathrm{d}u}{\mathrm{d}z} = \frac{\alpha}{L} u_s \tag{5}$$

in this relation, α is the slip coefficient, L is the length scale of the perforation, and u_s is the slip velocity.

Similar relations highlighting the slip velocity have also been obtained by Pozrikidis [29]. He considered many flows configurations: flow over a screen, sieve, planar solid matrix, thin slab, a periodic array of spheres, or infinite cylinders. These investigations were realized at very low Reynolds numbers corresponding to Stokes flows. Parallel shear flow on one side of the porous interface resulted in a slip velocity at the membrane's wet surface and a drift velocity parallel to the membrane on the other side. The drift velocity is roughly proportional to the slip velocity. The proportionality coefficient depends on the membrane thickness [29]. So, the drift velocity is equal to the slip velocity only in the case of a zero-thickness membrane. Computation of a shear flow past a permeable interface modeled as an array of cylinders by Pozrikidis [30] shows that both the direction and the magnitude of the slip and drift velocities depend on the interface characteristics, the porosity, and the Reynolds number. Pozrikidis [31] summarizes previous results from different authors of a laminar (low Reynolds number) shear flow over a solid surface containing perforations with several different types of surface modeling. The modeled surfaces were parallel slits, a surface with circular holes or square lattices, a doubly periodic array of spherical or spheroidal particles, a periodic array of cylinders, a doubly periodic array of square or circular plates with uniform gaps between each plate. Each of these configurations led to a different analytical expression of the slip velocity. This highlights the strong dependency of the slip velocity on the geometry of the surface. The author concluded that it was impossible to establish a universal law of the slip velocity. Pozrikidis [30] also investigated the effect of the Reynolds number on the slip velocity and concluded that inertial effects appearing at higher Reynolds numbers accentuate the magnitude of the slip velocity. However, since the flow at high Reynolds numbers is no longer governed by the linear Stokes equations but by the Navier-Stokes equations, it was impossible again to derive an analytical expression of the slip velocity.

The case where the flow is oblique toward the plate is less encountered. The numerical modeling of such flow requires accounting for the two effects: the pressure jump resulting from the traversing of the flow in the normal direction to the plate and the velocity deficit due to the tangential flow, which arises from the slip condition applying at the perforated surface. The first case was widely investigated, and analytical relations can be found in textbooks [7] and easily implemented. However, in the second case, it was shown from the above review that an easily implementable slip velocity relation could not be deduced. Moureh *et al.* [32] modeled pallet walls as pressure jump interfaces, neglecting the slip velocity effect, and reported significant differences between numerical and experimental results.

They attributed these differences to the fact that the tangential friction was not considered. In the same way [33] [34] and [35] modeled a perforated plate as a thin porous region with anisotropic permeability. In these studies, the interface conditions were not correctly modeled, which led to unsatisfactory results.

The above review shows the two canonical cases that are the most investigated: the flow tangential to a perforated plate/porous medium and the flow normal to a perforated plate/porous medium. The configuration where these two configurations are both encountered simultaneously is less studied.

This type of configuration can be encountered in refrigerated facilities of the cold chain. Palletized foods include vented pallets that combine perforated walls and macroscopic porous medium representing the stack. They are maintained at the right temperature by using a wall jet that diffuses inside the whole enclosure. Due to the complexity of the geometry, some regions will be characterized by a tangential flow over a perforated/porous medium and others by a flow normal to a perforated surface. In this type of configuration, previous numerical modeling of the perforated surface only considered the effect of the pressure jump through the perforated plate/porous medium, which led to unsatisfactory results [32].

This paper aimed to consider a simple configuration where the two phenomena can exist simultaneously: the normal pressure deficit through the plate and the velocity slip in the tangential direction. It also aimed to investigate how to account for the two effects during numerical modeling. Therefore, the transversal diffusion of a wall jet through a perforated plate placed inside an enclosure was considered. The configuration in which a porous medium (stack of spheres) is located below the perforated plate was also investigated.

This configuration allowed the investigation of the pressure jump through the plate and the slip velocity and their dependency on the perforated plate's geometry characteristics like the porosity, the shape of the pores, and the height of the clear region above the plate (*i.e.*, the velocity profile).

The investigation was realized by determining the airflow pattern and the enclosure's mean and fluctuating velocity profiles. Firstly, the flow in the empty enclosure was investigated. After that, the influence of the perforated plate, the effect of the plate porosity, the impact of the plate's position relative to the jet slot inlet, and the influence of the porous medium were studied.

2. Experimental Device

2.1. Geometry of the Enclosure

The experiments were carried out using the enclosure shown in **Figure 1**. The blowing and the outlet sections are located on opposite sides. The air is supplied through a rectangular inlet section of height 5 cm tangential to the ceiling. The enclosure height was 75.5 cm, the length was 400 cm, and the width was 37.6 cm. The wind tunnel is a closed-loop facility. The exit of the geometry is designed like a convergent to facilitate the numerical modeling of the geometry. The convergent design of the exit tends to create a positive pressure gradient between the

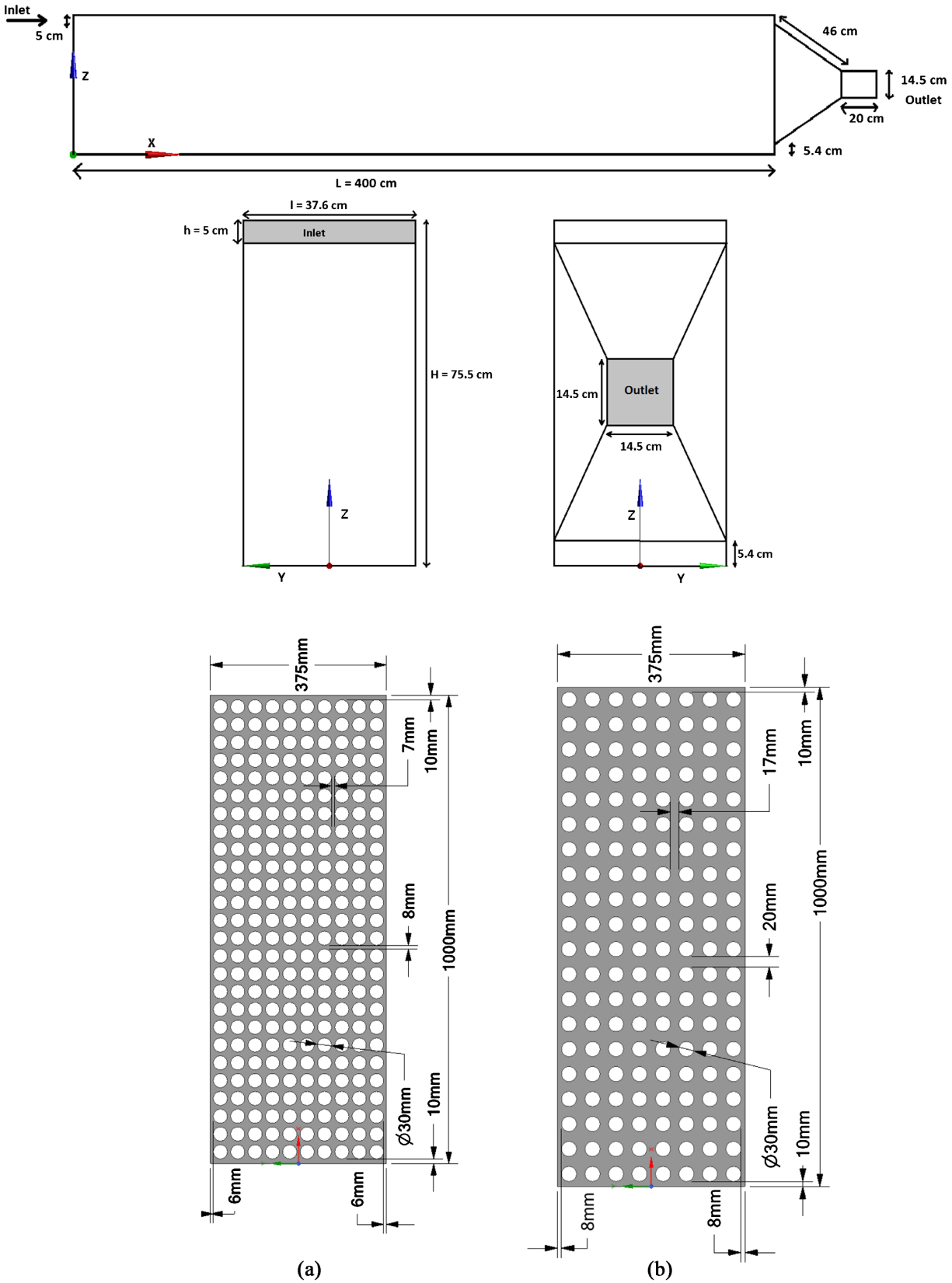

Figure 1. Schematic view of the empty enclosure and the perforated plates. (a) Perforated plate of thickness $t = 4$ mm and porosity of $\phi = 0.5$; (b) Perforated plate of thickness $t = 4$ mm and porosity of $\phi = 0.3$.

exit and the first part of the enclosure, which stabilizes the numerical simulation.

The inlet airflow rate was $Qu_0 = 1516\ \mathrm{m^3/h}$, corresponding to an inlet velocity of $U_0 = 22.4\ \mathrm{m/s}$. The hydraulic diameter was $D_0 = 8.83\ \mathrm{cm}$, and the kinematic viscosity was $\nu = 1.5\times10^{-5}\ \mathrm{m^2/s}$. The resulting inlet Reynolds number based on the hydraulic diameter, the inlet velocity, and the kinematic velocity was $R_0 = D_0U_0/\nu = 1.3\times10^5$. All the model's walls were made of wood except one lateral face, made of glass to allow internal air velocity measurement using a two-dimensional Laser Doppler Anemometer (LDA).

2.2. Geometry of the Perforated Plate and Porous Medium

Two perforated plates with porosities of $\phi = 0.3$ and $\phi = 0.5$ were utilized to investigate the influence of the porosity on the velocity difference at the interface. The plates are shown in **Figure 1**. The diameter of the holes is $d_h = 3\ \mathrm{cm}$ in all configurations. The thickness of the plates is $t = 4\ \mathrm{mm}$. Two heights were chosen to study the influence of the position of the plates on the flow structure: $Z = 60.5\ \mathrm{cm}$ and $Z = 50.5\ \mathrm{cm}$ (position of the upper face of the plate) *i.e.*, 10 cm and 20 cm below the jet entrance.

The porous medium was a stack of spheres of a diameter of 3.75 cm (ping-pong balls). It extended along the whole enclosure and toward both lateral walls. Its height was 20 cm. The top of this porous layer was located 10 cm below the perforated plate.

2.3. Laser Doppler Anemometer (LDA)

The LDA system was a Dantec Dynamics technology. The system could correctly resolve the sign of the velocity, the magnitude, and the fluctuations. The system comprised a 70 mW laser diode, emitting a visible red beam at a wavelength of 660 nm and an infrared beam at 785 nm wavelength. A beamsplitter enabled splitting the incident beam into two beams with the same characteristics. One of the split beams went through a Brag (acousto-optic) cell, shifting its frequency, allowing negative velocity resolution. A focusing lens of 50 cm was used to create a measurement volume resulting from the crossing of the two split beams. A receiving lens of 50 cm and a pinhole arrangement allowed the collection of light scattered by the moving particles. The emitting and the receiving optics were merged into one optic system. An oil atomizer producing particles with a diameter of about 4 μm was used. The seeding is realized in a plenum chamber situated upstream from the inlet slot. The accuracy is considered to be below 0.1% [36]. Thanks to this setting, vertical, longitudinal, and transversal velocity profiles were realized throughout the enclosure.

A maximum of 10,000 samples was specified for each point measured during these measurements, with a maximum sampling time of 120 s. The data acquisition was stopped according to which of these two events occurred first. The data rate varied between 500 and 5000 Hz for all measurements.

The probe was positioned by a computer controlling a three-dimensional dis-

placement system that provides a resolution of ±0.5 mm in three directions.

3. Results and Discussion

3.1. Empty Enclosure

This section presents the airflow pattern in the empty enclosure. The results were deduced through mean and fluctuating velocity measurements

3.1.1. Overall Airflow Description

The transversal profiles of the mean longitudinal velocity component measured throughout the enclosure at mid-height of the inlet slot were conducted. A small effect of the lateral walls on the velocity profiles was observed, particularly near the inlet slot. Nevertheless, velocity profiles with greater uniformity were obtained as we moved downstream from the inlet slot. Consequently, data measurements for this investigation were realized in the symmetry plane, where the lateral wall effects were reduced.

Figure 2 depicts LDA measurements concerning the evolution of the velocity profile throughout the enclosure. In Figure 2(a), are represented field of velocity vectors. Approximately one measurement point out of 3 is considered in order to have better visibility. In Figure 2(b), we superimposed the contour of the longitudinal mean velocity (color scale from −8 to 24 m/s) on the streamlines. These figures highlight the existence of two recirculation zones. Downstream from the jet inlet slot, the jet spreads out by diffusion, which causes an increase in the mass flow of the jet via an entrainment mechanism. This process continues until the jet separation at the ceiling, which splits the jet into different airflow

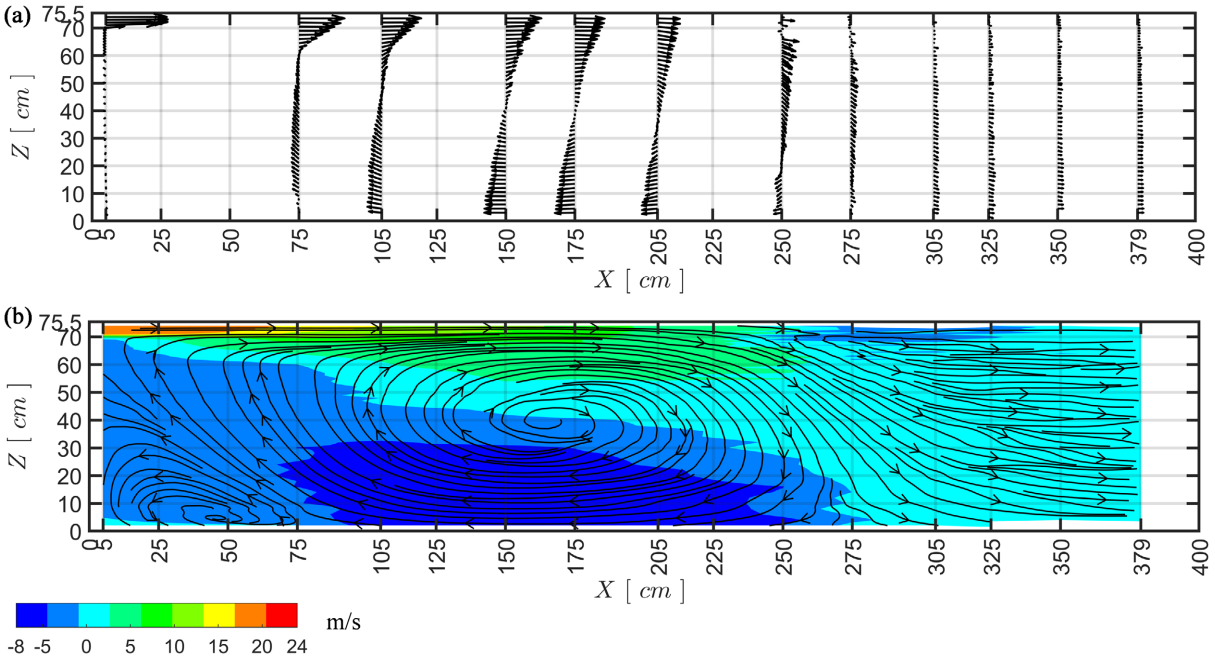

Figure 2. Airflow pattern of the mean flow: (a) velocity vectors, and the corresponding b) contour of the longitudinal velocity component (U) superimposed on the streamlines. (a) 2D velocity vectors using Laser-Doppler measurements (80 points); (b) Streamlines superimposed with the contour of the longitudinal component of the velocity (U).

components. The downstream part of the jet, which corresponds to the jet's mass flow rate (Qu_0), is drawn into the nozzle exit to continue the steady flow operation of the jet. The inner part is spilled back and entrains the formation of two recirculation zones into the enclosure. The main one is clockwise and extends from the inlet up to $X = 275$ cm, whereas the secondary recirculation is counterclockwise and is located in the enclosure's left and bottom part. This recirculation is similar to that appearing in backward-facing step flow configurations. The main recirculation results from separation at the ceiling level, giving rise to a negative longitudinal velocity in this area (**Figure 2**). The geometrical configuration of the enclosure exit entails a favorable pressure gradient responsible for the separation at the ceiling. This phenomenon has already been seen in previous investigations of room air ventilation [37]. Jin and Ogilvie [38] investigated an enclosure similar to the present configuration. The inlet and the outlet were opposite each other (on the right and left walls). They observed that this phenomenon (separation and recirculation) appeared when the incoming jet velocity was above a given value.

Hereafter, the wall jet characteristics are analyzed. These characteristics were compared with previous investigations of wall jets.

Figure 3(a) depicts the LDA vertical profiles of the longitudinal mean velocity (U), measured in the symmetry plane along the enclosure. Only the profiles upstream from the separation from the ceiling are shown. The mean velocity (U) is non-dimensionalized by the local maximum velocity of the profile (U_m) and the vertical coordinate (b). The latter is defined as the distance from the wall, where the velocity is equal to half the maximum velocity of the profile ($b = \bar{Z}$) where ($U = U_m/2$). Non-dimensional representation of the mean velocity profiles allows comparison with the empirical formula of Verhoff [39]. It describes the evolution of a two-dimensional wall jet's mean velocity profiles along the jet axis. Experimental data exhibit good agreement, suggesting the development of a two-dimensional wall jet in the empty enclosure.

Figure 3(b) presents the decay of the maximum velocity U_m along the enclosure in the dimensionless form: $(U_0/U_m)^2$ is plotted as a function of (X/h) to compare with literature data. The graph exhibits the existence of three different regions. The first region ($0 < X/h < 10$) corresponds to the potential core where the mean velocity is constant and is equal to the jet exit velocity. The second region ($10 < X/h < 35$) is the development region where velocity profiles are self-similar, as shown in **Figure 3(a)**. The third one extends beyond $X/h = 35$. **Figure 3(b)** also shows that the maximum velocity in the same section is lower in the current experimental data than that observed by Rajaratnam *et al.* [40] or by Yu *et al.* [41] in a confined enclosure, where the inlet and the outlet sections were located on opposite walls. This difference could be explained by the effect of the jet separation occurring at the downstream coordinate ($X/h = 55$). A better fit with the current experimental data was found with the experimental data of [42], where the inlet and the outlet sections were located on the same face.

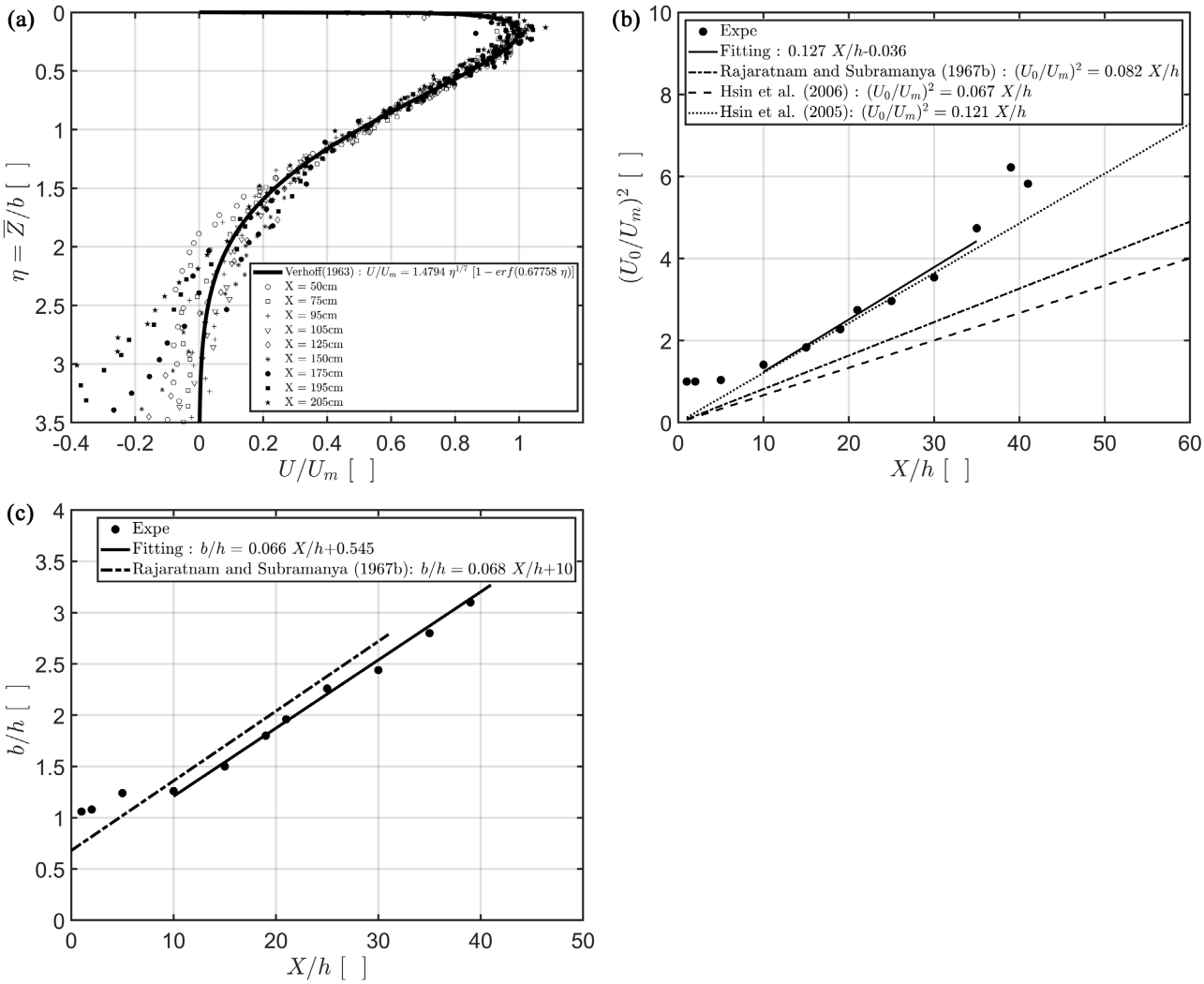

Figure 3. Characteristics of the confined wall jet. (a) Comparison of normalized velocity profiles with empirical velocity profile of a wall jet; (b) Evolution of $(U_0/U_m)^2$ with the normalized distance from the inlet section; (c) Evolution of the normalized thickness of the wall jet.

Figure 3(c) presents the evolution of the dimensionless thickness (b/h) along the enclosure. The spreading of the jet appears quite similar to that observed by Rajaratnam *et al.* [40].

3.1.2. Velocity Evolution along the Jet Axis

Figure 4 depicts the evolution of mean and fluctuating velocity measured along the jet axis (in the symmetry plane at mid-height of the inlet slot). The evolution of the longitudinal mean velocity exhibited three zones. The first one was located near the inlet ($0 < X < 20$ cm) corresponding to the potential core and was characterized by a constant velocity. The second zone extended between $X = 20$ cm and $X = 200$ cm , characterized by a constant slope.

This region corresponds to the region where vertical profiles of mean velocity are similar. The third zone extended between $X = 200$ cm and the separation position located at around $X = 275$ cm and was characterized by a steeper

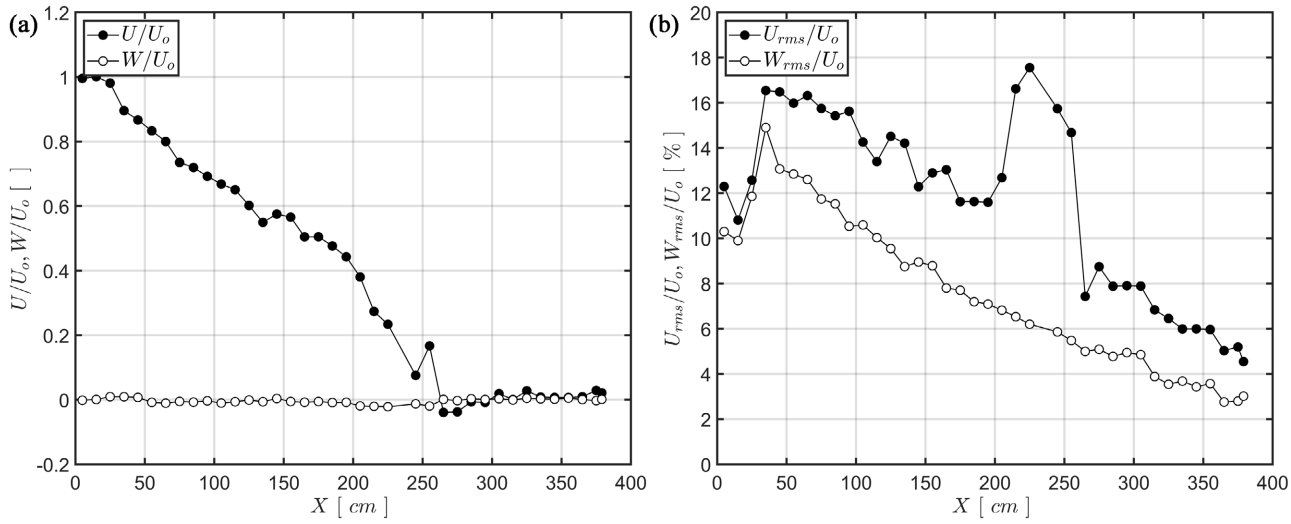

Figure 4. Evolution of mean velocities and fluctuating velocities along the jet axis (at 2.5 cm from the wall). (a) Mean velocities; (b) Fluctuating velocities.

slope. Downstream from the separation position at $X = 275$ cm, the longitudinal velocity initially exhibited some negative values and then remained very low. As mentioned in the above section, the flow separation was caused by the adverse pressure gradient in the rear part of the enclosure. It could not be counteracted by the inertia of the jet, whose velocity had become too low. It then appears that the slope change between the second zone and the third zone denoted the influence of the positive pressure gradient. A higher inlet air-jet velocity will tend to expand the length of the second zone.

Concerning the mean vertical velocity, it appeared to be constant, positive, and very low along the whole length of the enclosure.

In **Figure 4(b)**, the normalized root mean square of the velocity fluctuations in longitudinal and vertical directions $\left(U_{rms}/U_0, W_{rms}/U_0\right)$ are plotted. We can first notice that the turbulence intensity of the longitudinal velocity is much higher than the turbulence intensity of the vertical velocity. This tendency shows the high degree of anisotropy between the two components. This could explain the better ability of the RSM model to simulate the wall jet flows compared to k-ε or k-ω models ([37] [43]). The RSM model accounts for the anisotropy of the Reynolds stress to a greater extent.

At around $X = 275$ cm, where separation occurs, the longitudinal velocity component exhibits a high turbulence peak, which could be associated with the unsteadiness of the separation zone.

3.2. Enclosure with a Perforated Plate

This section presents the influence of the perforated plate on the mean airflow pattern and the turbulence intensity distribution in the enclosure.

3.2.1. Overall Airflow Description

A comparison of airflow patterns between the empty enclosure and the configu-

rations with perforated plates of porosity $\phi = 0.3$ or $\phi = 0.5$ located at $Z = 60.5$ cm (top of the plate) is represented in Figures 5(a)-(c). The comparison highlights the strong influence of the plate, whatever its porosity.

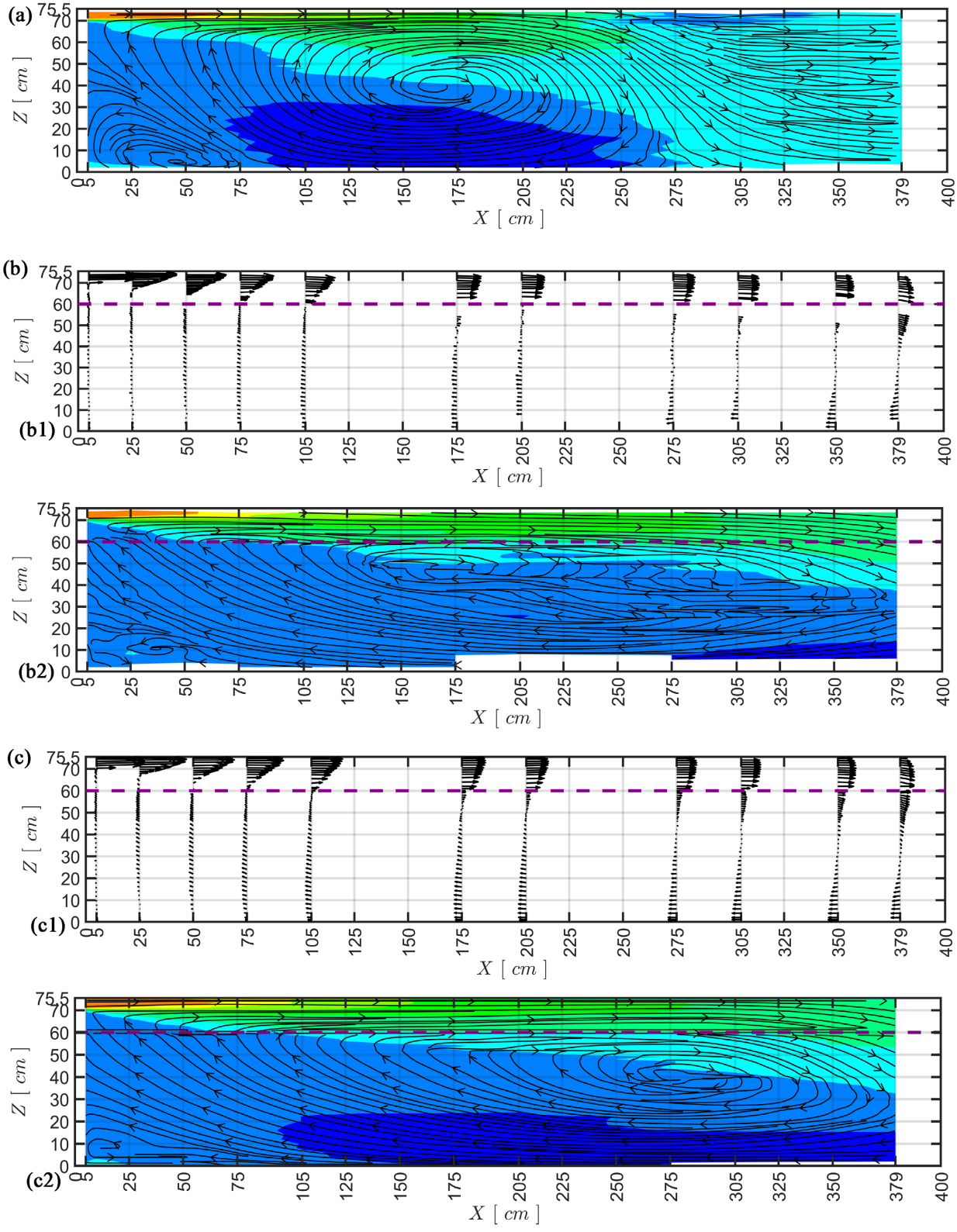

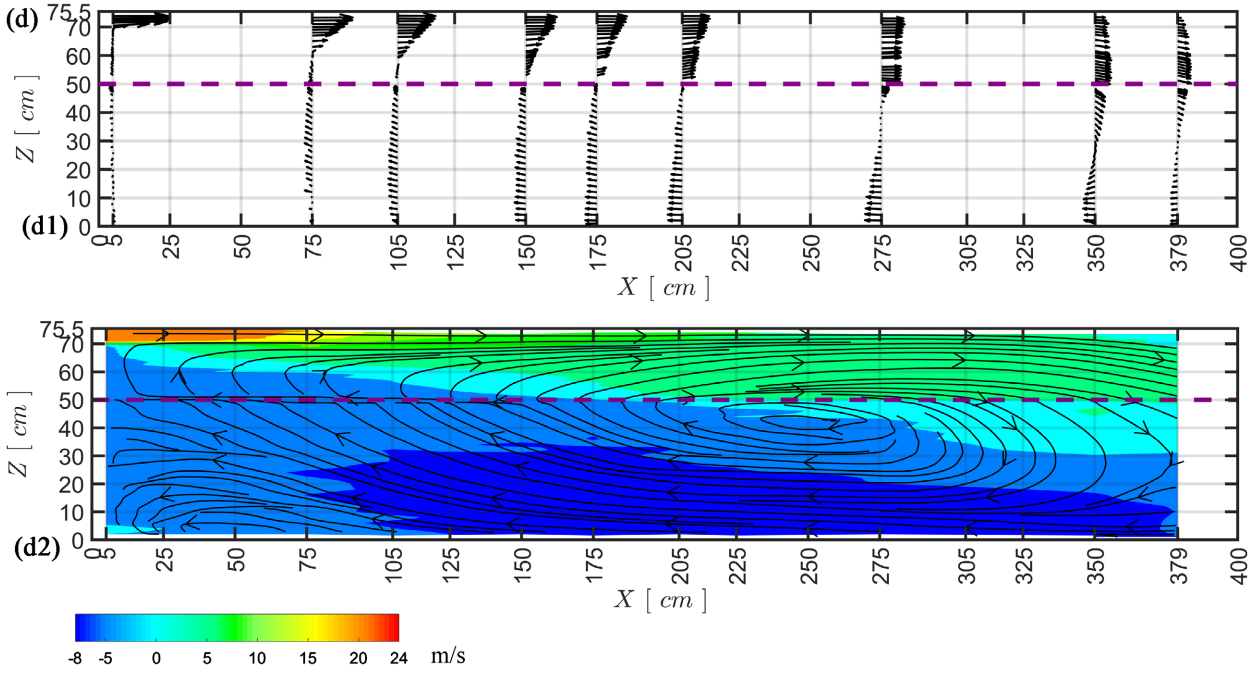

Figure 5. Comparison of the mean flow organization between configurations of empty enclosure and the three perforated plate cases: $Z = 60.5$ cm - $\phi = 0.3$, $Z = 60.5$ cm - $\phi = 0.5$ and $Z = 50.5$ cm - $\phi = 0.5$. (a) Empty enclosure; (b) Perforated plate— $Z = 60.5$ cm - $\phi = 0.3$; (b1) 2D velocity vectors using Laser-Doppler measurements (100 points); (b2) Streamlines superimposed with contour of longitudinal component of the velocity (U); (c) Perforated plate— $Z = 60.5$ cm - $\phi = 0.5$; (c1) 2D velocity vectors using Laser-Doppler measurements (100 points); (c2) Streamlines superimposed with contour of longitudinal component of the velocity (U); (d) Perforated plate— $Z = 50.5$ cm - $\phi = 0.5$; (d1) 2D velocity vectors using Laser-Doppler measurements (100 points); (d2) Streamlines superimposed with contour of longitudinal component of the velocity (U).

Near the inlet slot, the jet behaves similarly for all configurations. The jet spreads out via a diffusion mechanism downstream from the jet nozzle inlet. At around $X = 75$ cm, the outer mixing layer of the jet starts interacting with the perforated plate. Downstream from this position the inner layer characterized by higher velocities interacts with the perforated plate at around $X = 100$ cm. This position can be considered where the jet flow starts interacting with the perforated plate. From this position, the jet flow is partly confined by the perforated plate, which strongly limits the vertical diffusion of the jet through the plate while reinforcing the horizontal flow. Consequently, the jet separation on the ceiling observed in an empty configuration is ultimately delayed, implying less curvature in the streamlines entering the whole enclosure. Moreover, the flow recirculation center is shifted further downstream towards the rear part of the enclosure. Nevertheless, no significant differences were seen in the flow structure relative to the perforated plate porosities.

Figure 5(d) presents the flow pattern when the perforated plate of porosity $\phi = 0.5$ is positioned at $Z = 50.5$ cm. It is similar to the other configurations (with the plate positioned at $Z = 60.5$ cm). The flow mainly circulates in the region located above the perforated plate. The main difference is the region where the jet reaches the perforated

plate positioned at $Z = 60.5$ cm compared to that positioned at $Z = 50.5$ cm since the jet continues to spread until it reaches the perforated plate.

3.2.2. Vertical Velocity Profiles

Figure 6 depicts a comparison of vertical profiles of longitudinal mean velocity, along the enclosure, between the empty enclosure case and the three perforated plate cases. First, the cases where the plate was positioned at $Z = 60.5$ cm (red curves) with two porosities 0.3 and 0.5 are discussed.

In the first sections downstream from the inlet slot, similar wall jet behavior was observed for all cases (Figures 6(a)-(c)). The wall jet spreads out freely in the wall-normal direction towards the surrounding fluid. At around $X = 100$ cm (Figure 6(c)), where the jet meets the perforated plate, we noticed the first discrepancies between the empty enclosure and the perforated plate configurations. A large part of the mass flow was blocked above the plate, resulting in a higher mass flow in this area compared to the empty case. The region above the plate behaves as a channel. The jet flow tended to evolve to a channel flow while exhibiting stronger gradients at the perforated plate interface than the empty case (Figures 6(d)-(f)).

Figure 7 depicts the mass flow rate calculated in the section situated above the plate ($Z = 60.5$ cm, $\phi = 0.5$) by integrating the mean velocity profile and assuming that the flow is uniform in the transversal direction. The curve shows an increase in the mass flow rate next to the jet entrance ($X < 100$ cm), corresponding to the region where the jet has not yet reached the perforated plate. This increase in the mass flow rate expresses the impact of the entrainment process in the mixing layer of the jet upon the surrounding fluid. In the region located between $X = 100$ cm and $X = 300$ cm , the mass flow rate decreased slightly before showing a more substantial decrease in the region situated beyond $X = 300$ cm . In the region located between $X = 100$ cm and $X = 300$ cm , even if the flow showed a channeling effect, vertical diffusion (downward velocity) takes place through the perforations of the plate, leading to a decrease in the mass flow rate. Finally, the substantial decrease in the mass flow rate beyond $X = 300$ cm is explained by the enclosure's geometry exit and the flow entrainment from the rear part to the front part of the enclosure.

At $X = 275$ cm , from the mass flow rate at this position $Q_u = 0.464\ \mathrm{m^3/s}$ (see Figure 7), one can deduce the bulk velocity $\overline{u} = 8.22\ \mathrm{m/s}$. Given the hydraulic diameter in this section, $D_h = 0.21$ m , the corresponding Reynolds number is $Re_D = \overline{u} D_h / \nu = 1.18 \times 10^5$. This high Reynolds number suggests that the flow is turbulent in this section. Thus, the velocity profile of the boundary layer, when non-dimensionalized, evolves as the logarithmic profile: $U^+ = 1/\kappa \times \ln\left(z/z^*\right) + C$, where $U^+ = U/u_\tau$, $u_\tau = \sqrt{\tau_w/\rho}$ is called friction velocity, τ_w is the wall shear stress, and $\kappa = 0.41$ is the Von Karman constant for a smooth wall. $z^* = \nu/u_\tau$ and $C = 5.4$. z^* and C depend on the rough wall's asperities (size, geometry).

Figure 8 shows the velocity profile at $X = 275$ cm for the perforated plate of

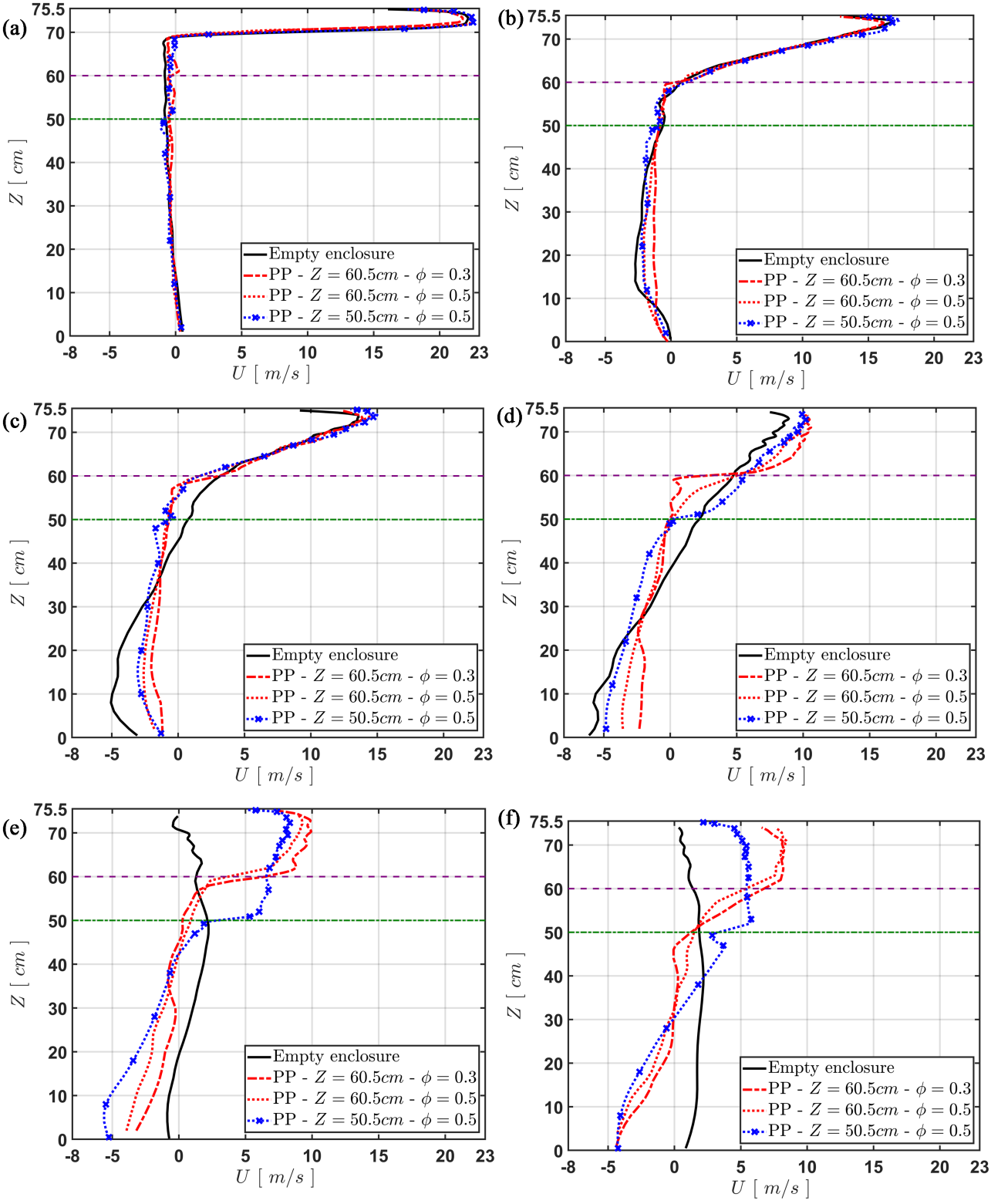

Figure 6. Effect of the perforated plate on the mean flow velocity profiles along the enclosure. (a) $X = 5$ cm ; (b) $X = 75$ cm ; (c) $X = 105$ cm ; (d) $X = 205$ cm ; (e) $X = 275$ cm ; (f) $X = 350$ cm .

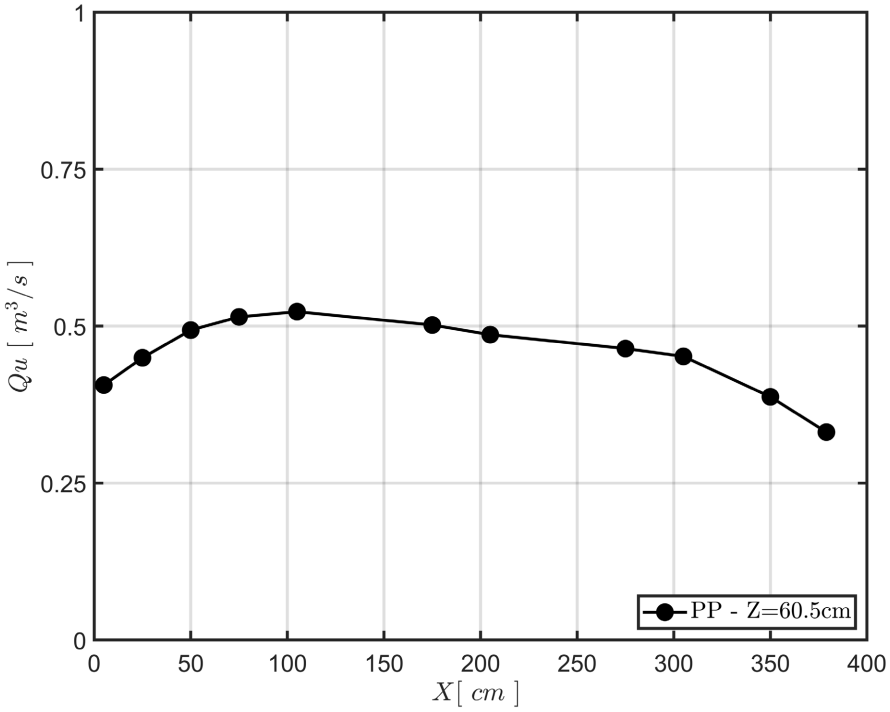

Figure 7. Mass flow rate (integration of the positive values of (U) in the section located above the plate ($Z \geq 60.5$ cm, $\phi = 0.5$) along the enclosure.

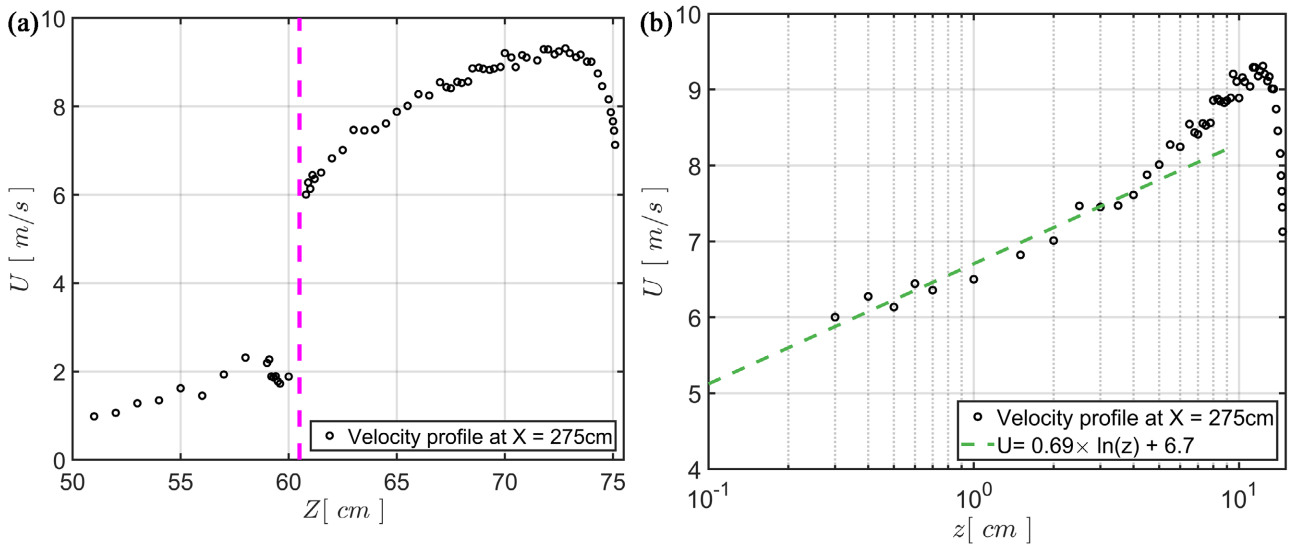

Figure 8. Linear U vs Z. (a) and semi-logarithmic U vs $\ln(z)$ (b) representations of the mean velocity profile above the perforated plate at section $X = 275$ cm.

porosity $\phi = 0.5$ (**Figure 8(a)**). It is superimposed with a semi-logarithmic representation of the velocity profile above the perforated plate: U versus $\ln(z)$ where z is the distance from the upper surface of the plate (**Figure 8(b)**). It seems that the behavior near the plate ($0 < z < 5$ cm) is almost linear. This confirms that the profile corresponds to a fully developed turbulent boundary layer. Schlichting [44] states that the slope corresponds to the friction velocity:

$u_\tau = \sqrt{\tau_w/\rho}$ divided by the von Karman constant. In this manner, regression makes it possible to determine the wall shear stress τ_w.

For $X = 275$ cm, the regression ($0.3\text{ cm} < z < 5\text{ cm}$) leads to $u_\tau = 0.283$ m/s and $\tau_w = 0.10$ Pa. From u_τ, it is also possible to estimate the characteristic distance $z^* = \nu/u_\tau$. The thickness of the laminar sublayer ($5z^*$) is thus about 0.2 mm. Since the first measurement position is $z = 3$ mm, it is clear that we could not determine the velocity in the vicinity of the plate to estimate a slip velocity. The logarithmic profile should typically apply between $20z^*$ and $200z^*$, that is from 4 to 40 mm.

Another way to estimate the shear stress is to consider the channel above the perforated plate to a rectangular duct. Thus, the shear stress is given by the following relation:

$$\tau_w = F_a \frac{1}{2}\rho\bar{u}^2 \tag{6}$$

where F_a is the Fanning friction factor and $\bar{u}$ is the bulk velocity in the channel above the plate.

The Reynolds number in section $X = 275$ cm is $Re_D = \bar{u}D_h/\nu = 1.18\times10^5$. For a smooth pipe at this Reynolds number, the Fanning friction factor based on the hydraulic diameter is 4.38×10^{-3}, leading to an estimation of wall shear stress of 0.18 Pa. It appears that the wall shear stress on the perforated plate estimated from the slope of U versus $\ln(z)$ is about 55% lower than the wall shear stress on a smooth plate. This suggests that the perforations of the wall lead to a decrease in the wall shear stress compared to a smooth plain plate. In the present configuration, the shear flow at the plate level arises from two distinct contributions. On the one hand, the contact area with the air is lower for a perforated plate, decreasing the average shear stress. On the other hand, the perforations resemble roughness, and this tends to increase turbulence in the vicinity of the plate and the wall shear stress in accordance with results obtained by [45] [46] and [47]. For $X = 275$ cm, where the flow in the channel is well developed, almost parallel to the plate ($|W| \ll U$), it seems that the first effect that promotes a reduction in wall shear stress is dominant.

Below the plate, the area near the wall is characterized by low velocities (low Reynolds numbers) in comparison to the mean velocity above the plate. Consequently, it can be expected that the flow will not be turbulent in this region. This leads to a wall shear stress lower than that on the upper wall of the perforated plate.

The flow is blocked in the upper channel, which entails a lower mass flow rate in the lower channel. Consequently, a substantial velocity difference between the upper and the lower region relative to the plate's position is noted as well as a shear stress jump (velocity gradient) (**Figures 6(d)-(f)**). This trend confirms previous low Reynolds number investigations of flow over a perforated plate/porous medium [9] [31].

In **Figure 6**, a slight difference between the two porosity cases (curves in red)

is seen when the jet flow interacts with the perforated plate. The flow velocity in the region above the plate is also lower for the higher porosity configuration. The vertical diffusion and the downward flow through the plate ($W < 0$), which are more straightforward in a plate with higher porosity, could explain this. Therefore, the flow rate above the plate decreases to a greater extent and takes place sooner.

The case where the plate is placed at $Z = 50.5$ cm (blue curves, **Figure 6**) is similar to the other configurations ($Z = 60.5$ cm) in the region located upstream from the position where the jet meets the plates. Downstream from this position, the velocity amplitude is lower above the plate since the section is more significant for approximately the same mass flow rate.

3.2.3. Turbulence Profiles

Vertical profiles of the longitudinal turbulence (in terms of a percentage of U_{rms}/U_0) are represented in **Figure 9**, where the empty enclosure and perforated plate configurations are compared.

First, the cases where the plate was placed at $Z = 60.5$ cm (red curves) are discussed for two porosities, 0.3 and 0.5. In the first sections, *i.e.*, upstream from the position where the jet meets the plate ($X < 100$ cm), an agreement between the cases can be observed, particularly in the region above the plate. A turbulence intensity peak is located in the mixing layer of the wall jet. This is in agreement with previous studies in the literature, where the position of the peak fluctuation is in the vicinity of the maximum value of the mean velocity gradient. This characterizes the development and the diffusion of the wall jet. This latter is realized via the thickening of the mixing layer. Consequently, the turbulence peak in the mixing layer thickens as we move in the longitudinal direction.

Downstream the position where the jet meets the plate, the overall fluctuating velocity level in the perforated plates configuration is reduced, compared to the empty enclosure in both regions located above and below the plate. This trend can be attributed to the suppression of the mixing layer development due to the presence of the plate, which limits the downward diffusion of the jet, and consequently develops as channel flow instead of jet flow. On the other hand, reducing vertical diffusion also reduces streamwise variations of the longitudinal velocity of the jet in its upper part, which reduces the amount of spatial velocity gradients of U and, therefore, the amount of turbulence generation. A peak in the velocity fluctuations is noticed near the perforated plate, reflecting the high-velocity gradient resulting from the boundary layer development through this perforated plate. This trend has been reported in previous studies of turbulent flow over a permeable wall [45] [48].

We can also notice a decrease in the fluctuating velocity between the regions above and below the plate for $X > 105$ cm . For example, the turbulence level in the region above the plate at $X = 205$ cm is about 7% compared with 4% below the plate. An initial explanation is that higher velocity magnitudes and gradients are encountered above the plate, so higher turbulence generation. A second

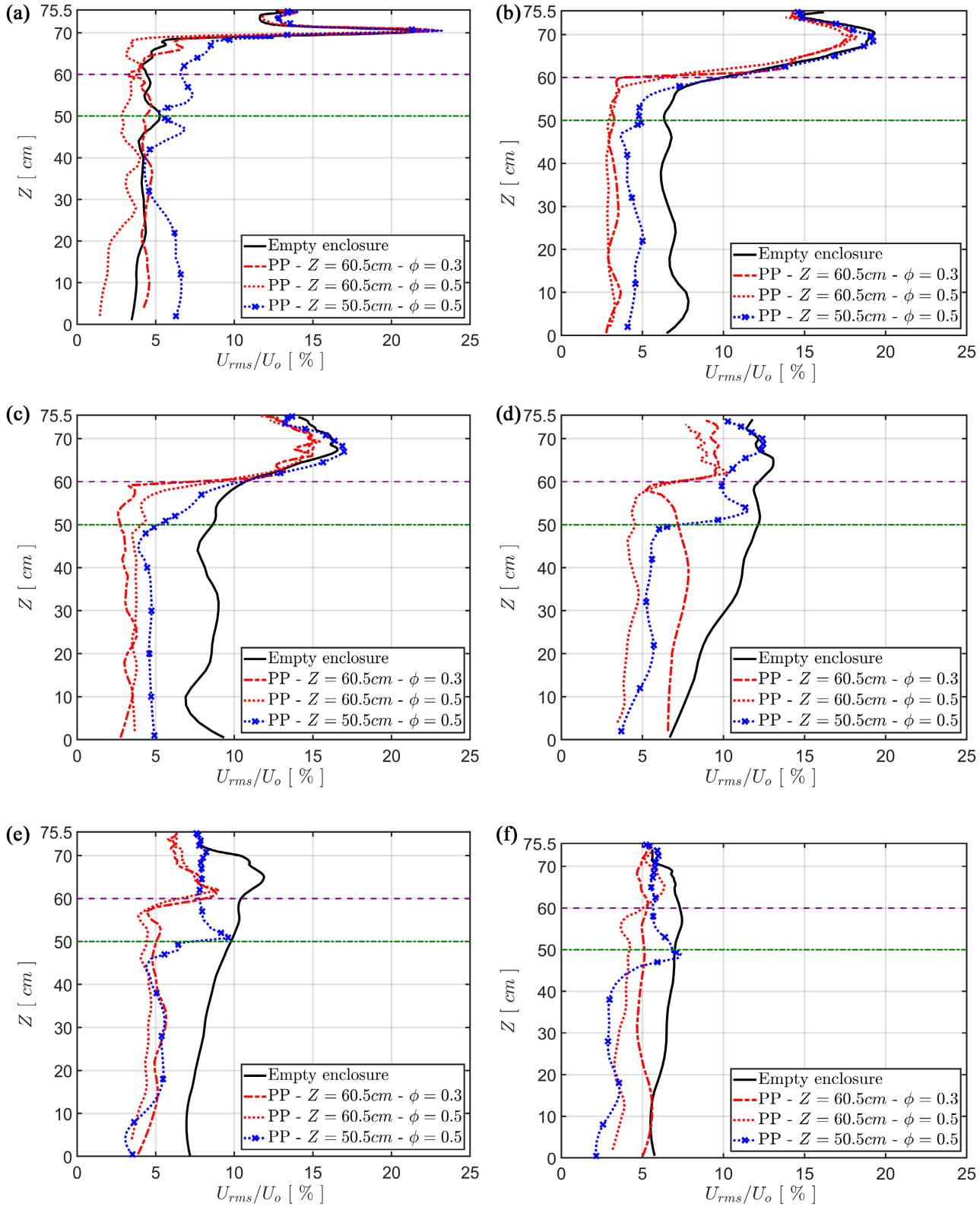

Figure 9. Effect of the perforated plate on the velocity fluctuation profiles along the enclosure. (a) $X = 5$ cm ; (b) $X = 75$ cm ; (c) $X = 105$ cm ; (d) $X = 205$ cm ; (e) $X = 275$ cm ; (f) $X = 350$ cm

explanation can be mentioned in the region where a downward flow occurs through the plate. On the one hand, flow through a perforated plate can generate turbulence; on the other hand, the perforated plate has a filtration effect on the turbulence. It acts as a threshold in the spectral space. Only eddies with a wave-number more significant than those associated with holes can traverse the perforated plate [49] [50].

In the plain plate vicinity, the viscosity effect leads to a damping of all the fluctuating velocity components up to zero at the wall level. In the current measurements, with the perforated plate, we could not verify such results. Measurements were not possible near the plate due to the reflection of the laser beams on the wall.

No significant differences could be seen between the two configurations with porosities of $\phi = 0.3$ and $\phi = 0.5$.

In the case where the plate is positioned at 50.5 cm (blue curves, **Figure 9**), we also clearly observed the turbulence intensity increase in the vicinity of the plate and the change in the fluctuating velocity level at the plate position (between the upper and the lower part of the plate). Here again, the perforated plate exhibited its filtrating effects on the fluctuating velocity.

3.2.4. Structure of the Flow at the Holes

This section presents a more detailed investigation of the flow structure at the level of the holes. **Figure 10(a)** and **Figure 10(b)** depict the superimposition of streamlines with turbulent intensity contours (in terms of percent of U_{rms}/U_0) measured below the plate, along the holes, and along the plain plate in the longitudinal direction. These measurements were realized between $X = 275\,\text{cm}$ and $X = 295\,\text{cm}$. The plain lines correspond to a 1D representation of the holes. Two situations arise from these representations. First, we noticed a downward flow developing as micro-jets through the holes, whereas we observed an upward flow along the plain plate. We saw the contribution of both the longitudinal and vertical velocity components. Just below the plate, between two successive holes, the velocity of the flow was approximately null (**Figure 10(a)**).

Further away from the plate, we observed a broadening of the widths of the jets with decreasing amplitude of the velocity vectors. This suggests a progressive merging of the jets as we move away from the perforated plate. Therefore, high-velocity gradients are encountered on the lower side of the plate due to the merging jets mechanism and the wavy character of velocity profiles, implying a high shearing area and high turbulence intensity. This turbulence is associated with the penetration effects of turbulent eddies through the pores, as already mentioned in above sections. The turbulence experienced a rapid decay as we move away from the plate.

Measurements along the wall show a different situation. The velocity vectors, as well as the streamlines, suggest ascending flow towards the wall. The flow appeared to be sucked towards the wall. This may result from the development of the micro-jets. In fact, it is clear that a micro-jet entails the entrainment of the

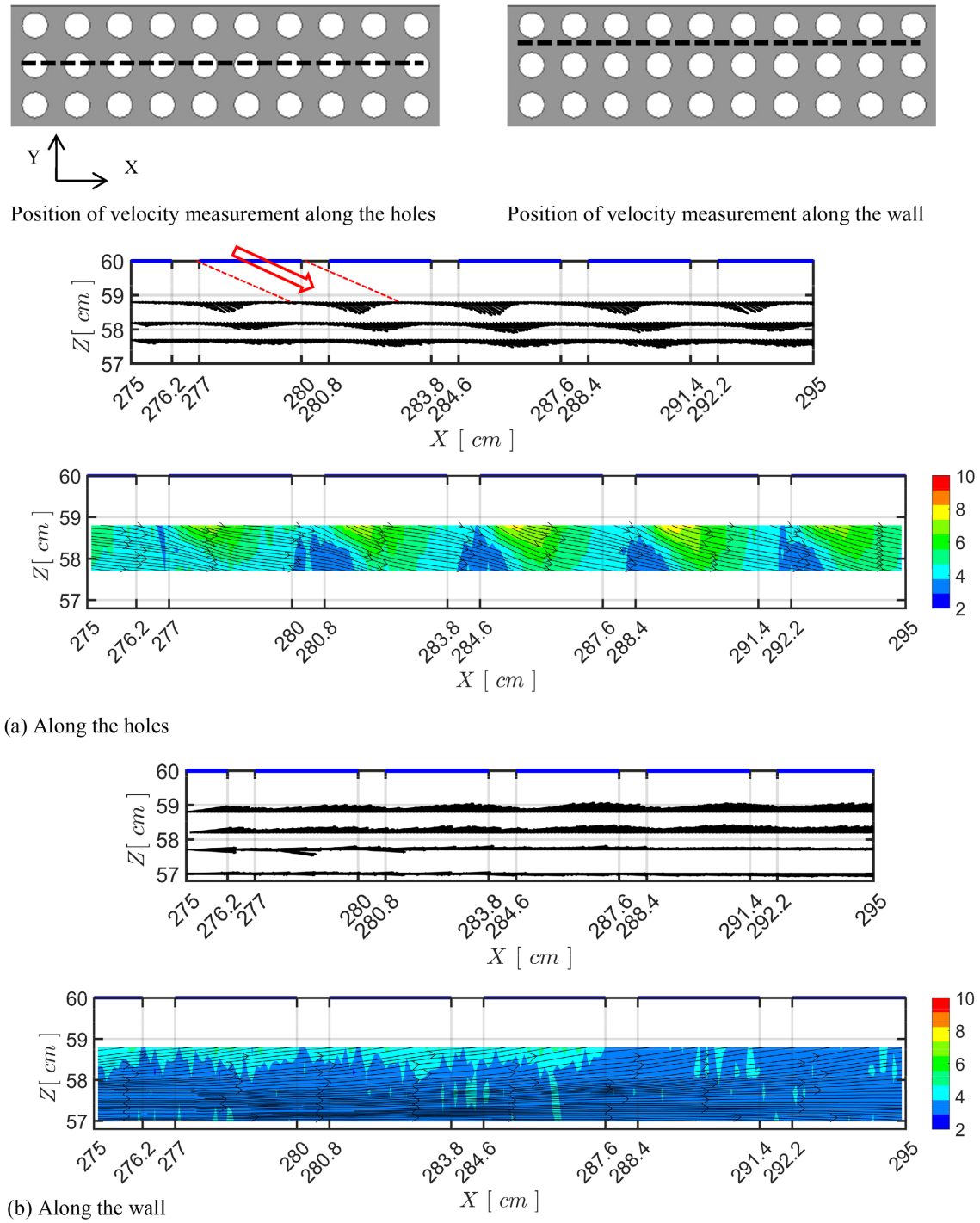

Figure 10. Longitudinal airflow pattern measured below the perforated plate of porosity $\phi = 0.5$ along the holes (a) and along the wall (b): field velocity vectors and superimposition of streamlines on turbulent intensity ($U_{rms}/U_0 \times 100$). (a) Along the holes; (b) Along the wall.

surrounding fluid. Consequently, the flow between two adjacent holes will be subjected to an entrainment process, leading to an ascending flow towards the wall. However, since the micro-jets merge far from the wall, the flow along the wall will first exhibit ascending vector velocity, which will progressively become

null, as seen in Figure 10(b). In the present case, unlike measurements along the pores, the superimposition of streamlines with turbulent intensity did not show any meaningful level. This confirmed the origin assigned to the turbulence in Figure 10(a).

Furthermore, we noticed a shift between the holes' positions and the micro-jets positions. This could be attributed to the measurements being realized at a distance of 1.2 cm below the plate and to the fact that the flow is convective in the longitudinal direction. This shift was present in the measurements along the wall and the holes.

Moreover, since the airflow pattern exhibited a recirculation extending throughout the entire enclosure (Figure 5), it is clear that the flow structure at the holes, as shown in Figure 10, is not identical everywhere. For example, in the vicinity of the jet entrance and around the exit of the enclosure, the flow traversing the perforated plate was more significant due to the jet entrainment process and the recirculation of the flow respectively. Velocity vectors near the entrance are oriented more vertically (in the direction of the positive Z-axis) than in the middle of the enclosure.

3.2.5. Mean Velocity Evolution above and below the Perforated Plate along the Enclosure

Figure 11 depicts the longitudinal profiles of the vertical velocity components measured at 2.5 cm above and below the perforated plate. We considered the perforated plate configurations with porosities of $\phi = 0.3$ and $\phi = 0.5$.

We have shown in the previous sections that the flow is ascending in the front part of the enclosure and descending in the rear part of the enclosure (see Figure 5, for example). In particular, in above sections, we deduced that the flow diffuses in the downward direction between $X = 275\,\text{cm}$ and $X = 295\,\text{cm}$ through the holes. In the same section, we also saw that the flow pattern is complex downstream from the perforated plate, with ascending and descending flow

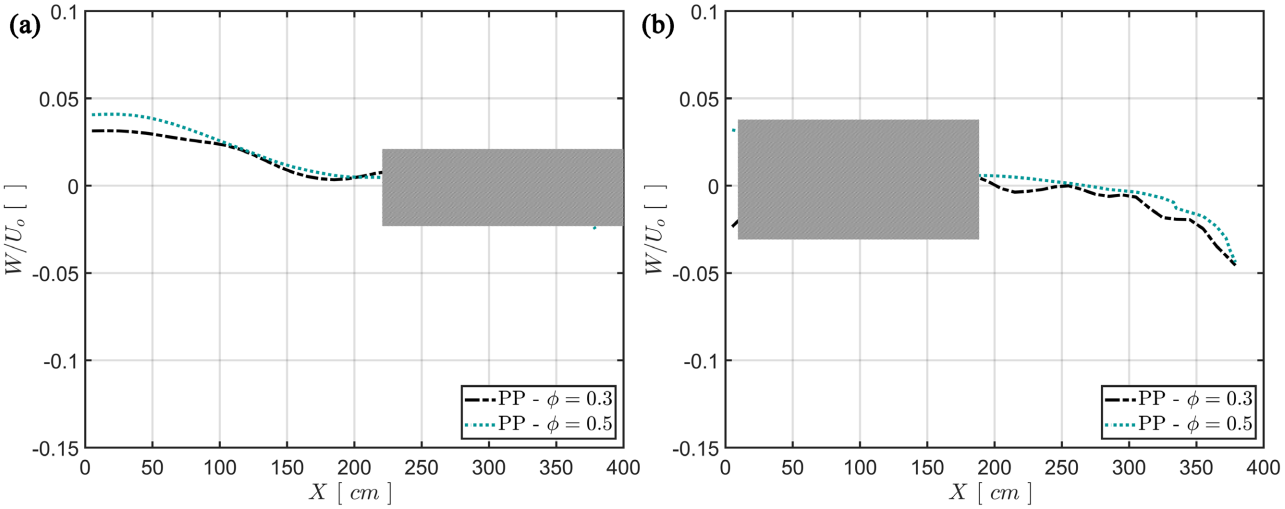

Figure 11. Comparison of vertical mean velocity profile along the enclosure. The perforated plate is placed at $Z = 60.5\,\text{cm}$. (a) Below the perforated plate (2.5 cm); (b) Above the perforated plate (2.5 cm).

areas. Therefore, the vertical velocity below and above the plate strongly depends on the exact measurement position in the rear part or the front part of the enclosure, respectively, leading to "noisy" profiles. This is why we considered the vertical velocity component upstream from the perforated plate: 2.5 cm below the plate for $X < 200$ cm and 2.5 cm above the plate for $X > 200$ cm.

It can be seen in **Figure 11(b)** that velocity profiles measured above the plate in the rear part of the enclosure are similar for the two perforated plate porosities. We noticed a slight difference at the entrance region in **Figure 11(a)**, which may be attributed to the entrainment process of the mixing layer of the jet. This entrainment process is affected by the perforated plate which behaves as an obstacle.

Knowing these shortcomings, we can deduce from these figures that, overall, the amplitude of the vertical velocity is lower for the perforated plate with a porosity of $\phi = 0.3$ compared with the perforated plate with a porosity of $\phi = 0.5$. This is acceptable since the lower porosity obstructs the flow to a greater extent and is consequently associated with a lower mass flow transfer through the plate.

Figure 12 presents the evolution of the longitudinal mean velocity measured 2.5 cm above and 2.5 cm below the plate. The plates (top of the plates) were placed at two different positions $Z = 60.5$ cm and $Z = 50.5$ cm, and had two different porosities, $\phi = 0.5$ or $\phi = 0.3$.

Next to the jet entrance, measurements show negative longitudinal velocity above and below the plate. These negative values reflect the recirculation of the flow and the entrainment process of the surrounding fluid. These negative values are followed by positive longitudinal velocity reflecting the convection of the flow in the longitudinal direction. Comparison between **Figure 12(a)** and **Figure 12(b)** shows that, above the plates, the velocity is higher for the plate with lower porosity. This results from the nature of the plate with the lower porosity, which is more efficient in preventing the flow from diffusing from the upper channel to the region below the plate, leading to a higher mass flow rate in the upper channel. The progressive increase in the velocity is linked to the progressive channeling of the flow along the upper channel. The flow enters the channel as a jet which diffuses throughout the entire section. The presence of the plate leads to a channeling effect exerted on the flow. The latter starts when the jet meets the plate at around $X = 100$ cm and $X = 175$ cm for the plates positioned at $Z = 60.5$ cm and $Z = 60.5$ cm. Let us specify that the size of the entrainment process (negative U) refers to the distance at which the mixing layer of the jet starts interacting with the plate. In the current figures, measurements were realized at a distance of 2.5 cm above the plate and 2.5 cm below the plate. Consequently, the position at which the mixing layer starts interacting with the plate should be between $X = 45$ cm and $X = 75$ cm for the configuration shown in **Figure 12(a)**.

The positive velocity below the plate denotes the drift velocity as noted by

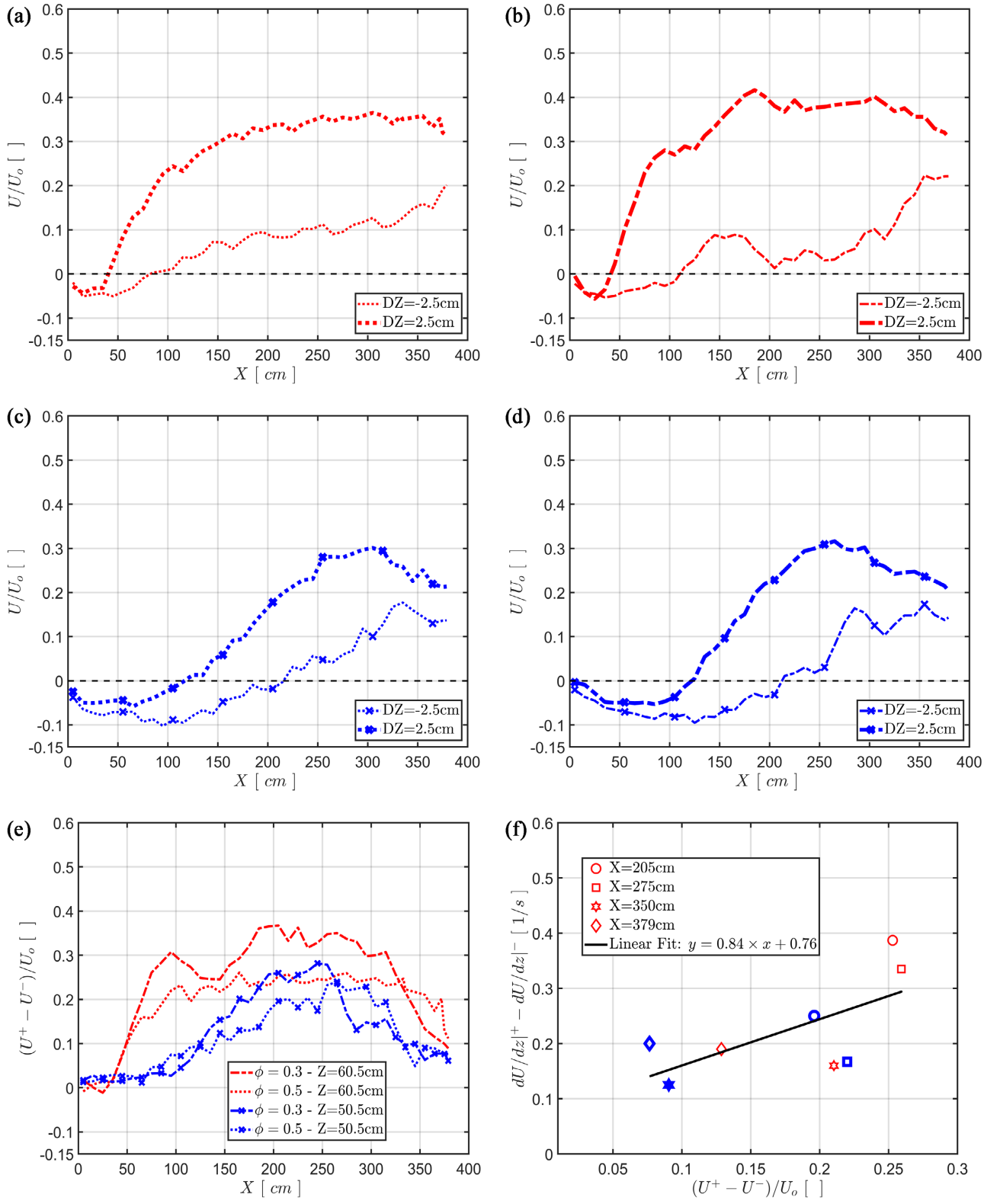

Figure 12. Velocity difference resulting from the presence of the perforated plate. (a) $\phi = 0.5$ - $Z = 60.5$ cm ; (b) $\phi = 0.3$ - $Z = 60.5$ cm ; (c) $\phi = 0.5$ - $Z = 50.5$ cm ; (d) $\phi = 0.3$ - $Z = 50.5$ cm ; (e) (f) $\phi = 0.5$.

[29], who states that a parallel shear flow on one side of an impermeable membrane resulted in a slip velocity at the membrane level and a drift velocity parallel to the membrane on the other side. The drift flow under the plate acts as a secondary wall jet entraining the surrounding fluid. Moreover, one can see from **Figure 6(d)** & **Figure 6(e)** that the drift velocity is strongly dependent on the porosity of the plate. A lower plate porosity, which is associated with a higher velocity in the region above the plate, leads to a lower drift velocity below the plate. The influence of the height of the section above the plate is more difficult to demonstrate.

Let us now consider the velocity difference just above and below the perforated plate (at ±2.5 cm). As stated in above sections, velocity measurements down to the viscous sublayer of the plate are not available; therefore, this velocity difference cannot be considered as slip velocity. Nevertheless, one could expect that an empirical boundary law could apply to this velocity difference. At first sight from **Figure 12**, we were able to conclude that it was not possible to deduce a universal law expressing the relationship between the velocity difference introduced by the plate and the porosity and/or the height of the cross-section above the plate, which confirms the conclusion of Pozrikidis [31] for low Reynolds number flows.

We utilized a wall jet diffusing vertically through a perforated plate in the present study. Moreover, the flow in the channel above the plate was not fully developed, which means that the flow configuration is strongly dependent on the longitudinal position. This is quite different from the configuration of flow over a porous wall described by [9], in which the flow in the clear medium was fully developed and was therefore dependent only on the height of the section and the characteristics of the lower permeable wall.

Overall, we can say that, for the same mass flow rate at the inlet, the velocity difference between the upper and the lower parts of the plate increases when the porosity decreases. We can also conclude that it increases when the height of the cross-section above the plate decreases. It is also clear that the velocity difference is related to the interaction between the jet and the plate, as can be seen in **Figure 12(e)**. In this figure, the plate positioned further from the jet inlet slot starts exhibiting a velocity difference at around $X = 100\text{ cm}$, whereas the closer one shows a velocity difference at around $X = 50\text{ cm}$.

The velocity difference above/below the perforated plate is logically related to the shear stresses above/below the plate, which are related to the shear rates ($\mathrm{d}U/\mathrm{d}z$). Therefore, we estimated the velocity gradient at 2.5 cm above/below the plate using the velocity profiles at several longitudinal positions ($X = 205\text{ cm}, 275\text{ cm}, 350\text{ cm}, 379\text{ cm}$) for $\phi = 0.5$ at $Z = 60.5\text{ cm}$ and $Z = 50.5\text{ cm}$, presented in **Figure 6**. **Figure 12(f)** presents the difference in shear rates versus the velocity difference (2.5 cm above/below the plate). They seem to be somewhat correlated in the region where the flow behaves as a channel flow, suggesting a relationship of the type expressed in Equation (7).

$$\left.\frac{\partial U}{\partial z}\right|_{+} - \left.\frac{\partial U}{\partial z}\right|_{-} = \xi(\phi)\left(U^{+} - U^{-}\right) \tag{7}$$

where the proportionality coefficient depends on the plate porosity.

In the configuration of a perforated plate with porosity $\phi = 0.5$ positioned at $Z = 60.5$ cm and $Z = 50.5$ cm, the proportionality coefficient $\xi(\phi)$ could be estimated at about 0.84 m^{-1}.

Further investigation should be conducted to confirm the pertinence of such a correlation.

3.3. Enclosure with a Perforated Plate and a Porous Medium

This section considers the configuration with a macroscopic porous region composed of a stack of spheres with a diameter of 3.75 cm (ping-pong balls). The porous bed was positioned in the region below the perforated plate ($Z = 60.5$ cm, $\phi = 0.5$), between $Z = 30$ cm and $Z = 50$ cm. In Figure 13, we superimposed streamlines on the contours of the longitudinal mean velocity for the configuration with and without a porous zone. Firstly, we can notice that the flow recirculation below the plate is shifted in the front part of the enclosure for the configuration with a porous zone. The center of the recirculation is located at around $X = 175$ cm in the presence of the porous medium and $X = 275$ cm without. These figures also showed that the longitudinal mean velocity in the region situated below the porous region was still negative, but its amplitude was lower than that without a porous medium. This indicates that the entrainment process in the mixing layer, which is responsible for the recirculation region, is

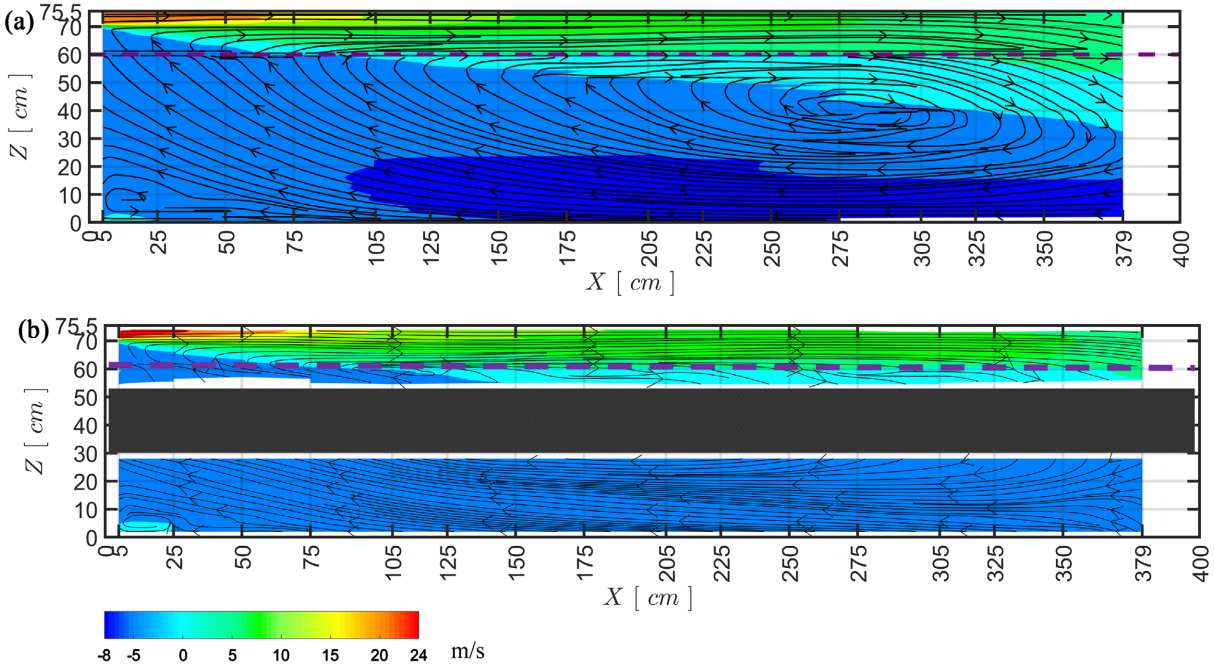

Figure 13. Comparison of the mean airflow pattern between configurations of the enclosure with the perforated plate (PP) and the configuration in which the perforated plate is associated with the porous medium (PP-MP). (a) PP configuration— $\phi = 0.5$; (b) PP-MP configuration— $\phi = 0.5$.

attenuated by the presence of the porous region.

The flow in the region below the macroscopic porous region is similar to that occurring in the region above the perforated plate. The flow is blocked in this region and behaves as a channel flow up to the enclosure's entrance. In this region, the flow is entrained toward the jet mixing layer. This behavior could be responsible for shifting the center of the recirculation toward the front part of the enclosure compared to the perforated plate case.

Figure 14 presents vertical profiles of the longitudinal mean velocity along the enclosure. Upstream from the position where the jet meets the perforated plate ($X = 100$ cm), the velocity profiles for both configurations show similar behavior. Downstream from this position, the amplitude of the mean velocity is reduced in the region situated above the perforated plate in the presence of the porous medium. Correlatively, the backflow in the region situated below the porous medium is also reduced. This is due to the mass flow conservation in each section.

These results show that the perforated plate and the macroscopic porous region have comparable effects on the flow. Therefore, this confirms that the perforated plate can be modeled as a thin porous medium. This result could be of great importance for numerical modeling of configurations where clear regions are adjacent to porous medium/perforated surfaces, such as in refrigerated trucks.

4. Conclusions

In this study, we carried out experiments to investigate the lateral diffusion of a confined wall jet through a perforated plate set in a longitudinal direction. We used LDA for velocity measurements throughout the entire enclosure. The influence of the perforated plate on the airflow pattern, the mean velocity, and the fluctuating velocity concerning the empty enclosure case was studied.

The airflow pattern was modified entirely compared to the empty enclosure configuration. The presence of the plate prevented the separation from the ceiling that takes place in the empty enclosure configuration.

The perforated plate acted on the fluctuating velocity as a filter to reduce its amplitude. This reduction arises from the suppression of the mixing layer development, which is the region of turbulence production, and from the holes allowing only small-scale turbulence eddies to pass through the perforated plate.

The results also show that the plate reduces exchanges between the upper and the lower sides. This limits the jet diffusion through the plate, leading to a more substantial channeling effect of the flow in the upper side of the plate with a higher mass flow rate.

Moreover, the results showed that the flow traverses the perforated plate as micro-jets that merge a short distance from the plate. The flow through the perforated plate is ascending near the entrance. In the middle of the enclosure, it is tangential to the plate. Finally, the flow descends towards the exit in the rear part.

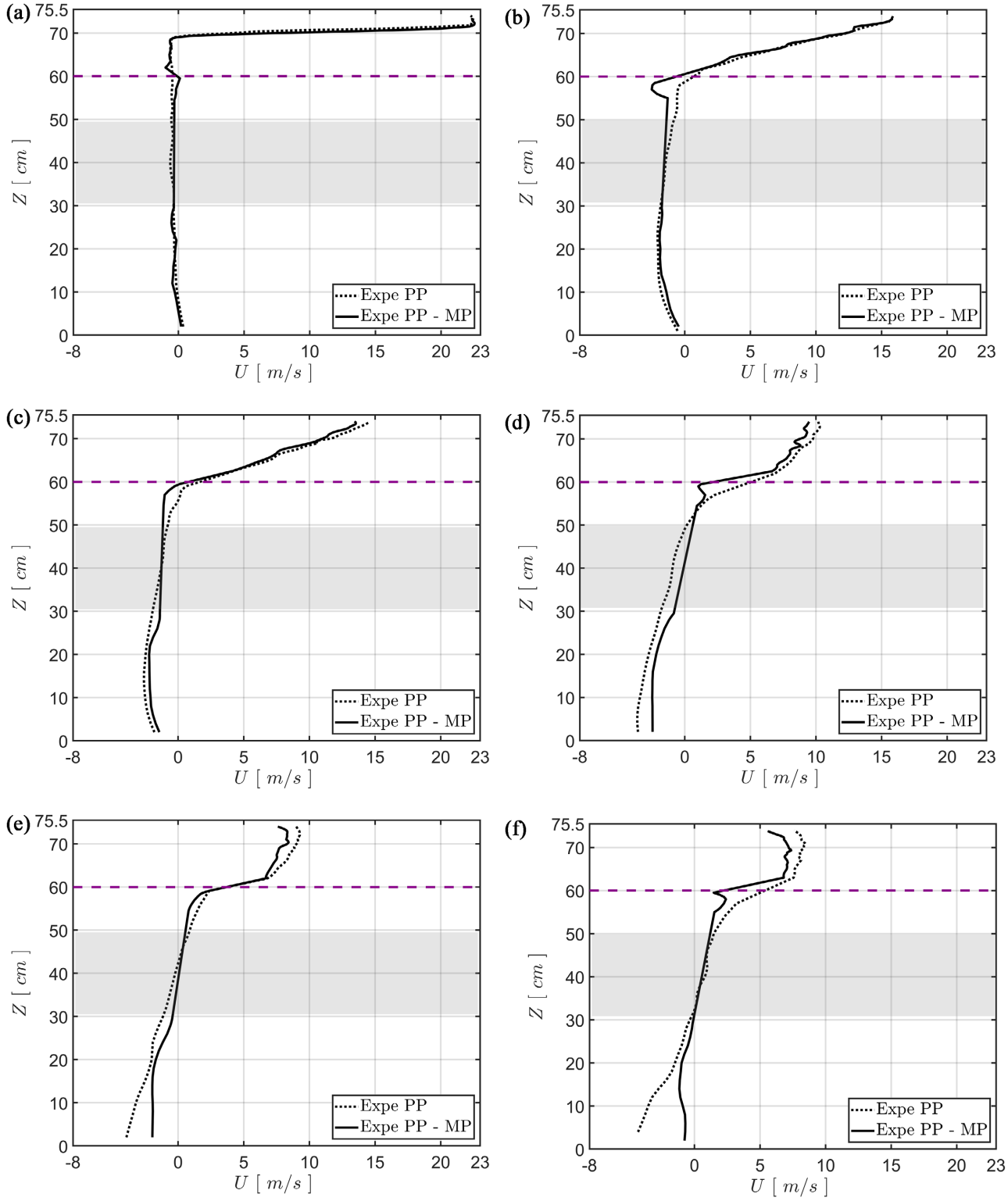

Figure 14. Effects of the porous medium on the mean flow velocity profiles along the enclosure in comparison with the effects of the perforated plate of porosity $\phi = 0.5$ placed at the position $Z = 60.5$ cm . (a) $X = 5$ cm ; (b) $X = 75$ cm ; (c) $X = 105$ cm ; (d) $X = 205$ cm ; (e) $X = 275$ cm ; (f) $X = 350$ cm .

Analysis of the velocity profiles near the perforated plate suggests that the perforations of the wall lead to a decrease in the wall shear stress by a factor of about 55% compared to a smooth plain plate. In the middle part of the enclosure, where the flow behaves as channel flow, experimental results derive a relationship expressing a correlation between the difference in shear rates and velocity at the two sides of the plate. The proportionality coefficient in this relationship depends on the perforated plate porosity and the height of the channel situated above the plate. It could also be inferred that this proportionality coefficient also depends on the perforations' shape, as indicated in the literature. Therefore, the difference in the velocities above and below the plates could not be related using a universal formula function of the geometric parameters. However, further investigation should be conducted to confirm the pertinence of such a correlation.

The case where a porous medium made of a stack of spheres is located under the perforated plate was also considered. The presence of the porous medium slightly decreased the velocities above the plate and the backflow under the porous zone. It seems that it limited the entrainment phenomena of the incoming jet.

Finally, the results from the two configurations of the perforated plate and the porous medium are similar, which entails that the perforated plate could be modeled as a thin porous medium.

Conflicts of Interest

The authors declare no conflicts of interest regarding the publication of this paper.

References

[1] Weber, L.J., *et al.* (2000) Headloss Characteristics for Perforated Plates and Flat Bar Screens.

[2] Erdal, A. (1997) A Numerical Investigation of Different Parameters That Affect the Performance of a Flow Conditioner. *Flow Measurement and Instrumentation*, **8**, 93-102. https://doi.org/10.1016/S0955-5986(97)00032-0

[3] Tullis, J.P. (1989) Hydraulics of Pipelines—Pumps, Valves, Cavitation, Transients. https://doi.org/10.1002/9780470172803

[4] Malavasi, S., Macchi, S. and Merighetti, E. (2008) Cavitation and Dissipation Efficiency of Multihole Orifices. In: Prague, C.Z., Zolotarev, I. and Horacek, J., Eds., *Flow-Induced Vibration*, Institute of Thermomechanics, Prague, 581-586.

[5] Malavasi, S., *et al.* (2012) On the Pressure Losses through Perforated Plates. *Flow Measurement and Instrumentation*, **28**, 57-66. https://doi.org/10.1016/j.flowmeasinst.2012.07.006

[6] Macchi, S. (2009) Analysis of Multi-Hole Orifices and Their Use in a Control Device. Dissertation.

[7] Idel'chik, I.E. (1966) Coefficients of Local Resistance and of Friction. U.S. Atomic Energy Commission and the National Science Foundation, Alexandria.

[8] Laplace, P. and Arquis, E. (1998) Boundary Layer over a Slotted Plate. *European Jour-*

nal of Mechanics—B/Fluids, **17**, 331-355.
https://doi.org/10.1016/S0997-7546(98)80262-8

[9] Beavers, G.S. and Joseph, D.D. (1967) Boundary Conditions at a Naturally Permeable Wall. *Journal of Fluid Mechanics*, **30**, 197-207.
https://doi.org/10.1017/S0022112067001375

[10] Saffman, P.G. (1971) On the Boundary Condition at the Surface of a Porous Medium. *Studies in Applied Mathematics*, **50**, 93-101.
https://doi.org/10.1002/sapm197150293

[11] Larson, R.E. and Higdon, J.J.L. (1986) Microscopic Flow near the Surface of Two-Dimensional Porous Media. Part 1. Axial Flow. *Journal of Fluid Mechanics*, **166**, 449-472. https://doi.org/10.1017/S0022112086000228

[12] Larson, R.E. and Higdon, J.J.L. (1987) Microscopic Flow near the Surface of Two-Dimensional Porous Media. Part 2. Transverse Flow. *Journal of Fluid Mechanics*, **178**, 119-136. https://doi.org/10.1017/S0022112087001149

[13] Richardson, S.A. (1971) A Model for the Boundary Condition of a Porous Material. Part 2. *Journal of Fluid Mechanics*, **49**, 327-336.
https://doi.org/10.1017/S002211207100209X

[14] Sahraoui, M. and Kaviany, M. (1992) Slip and No-Slip Velocity Boundary-Conditions at Interface of Porous, Plain Media. *International Journal of Heat and Mass Transfer*, **35**, 927-943. https://doi.org/10.1016/0017-9310(92)90258-T

[15] Brinkman, H.C. (1948) A Calculation of the Viscous Force Exerted by a Flowing Fluid on a Dense of Particles. *Applied Scientific Research*, **A1**, 27-34.
https://doi.org/10.1007/BF02120313

[16] Ochoa-Tapia, J.A. and Whitaker, S. (1995) Momentum Transfer at the Boundary between a Porous Medium and a Homogeneous Fluid—I. Theoretical Development. *International Journal of Heat and Mass Transfer*, **38**, 2635-2646.
https://doi.org/10.1016/0017-9310(94)00346-W

[17] Neale, G. and Nader, W. (1974) Practical Significance of Brinkman's Extension of Darcy's Law: Coupled Parallel Flows within a Channel and a Bounding Porous Medium. *Journal of Chemical Engineering*, **52**, 475-478.
https://doi.org/10.1002/cjce.5450520407

[18] Givler, R. and Altobelli, S. (1994) A Determination of the Effective Viscosity for the Brinkman-Forchheimer Flow Model. *Journal of Fluid Mechanics*, **258**, 355-370.
https://doi.org/10.1017/S0022112094003368

[19] Ochoa-Tapia, J.A. and Whitaker, S. (1995) Momentum Transfer at the Boundary between a Porous Medium and a Homogeneous Fluid—II. Comparison with Experiment. *International Journal of Heat and Mass Transfer*, **38**, 2647-2655.
https://doi.org/10.1016/0017-9310(94)00347-X

[20] Durlofsky, L. and Brady, J.F. (1987) Analysis of the Brinkman Equation as a Model for Flow in Porous Media. *Physics of Fluids*, **30**, 3329-3341.
https://doi.org/10.1063/1.866465

[21] Vafai, K. and Tien, C.L. (1982) Boundary and Inertia Effects on Convective Mass Transfer in Porous Media. *International Journal of Heat and Fluid Flow*, **25**, 1183-1190. https://doi.org/10.1016/0017-9310(82)90212-5

[22] Vafai, K. and Kim, S.J. (1990) Fluid-Mechanics of the Interface Region between a Porous-Medium and a Fluid Layer—An Exact Solution. *International Journal of Heat and Fluid Flow*, **11**, 254-256. https://doi.org/10.1016/0142-727X(90)90045-D

[23] Breugem, W.P., Boersma, B.J. and Uittenbogaard, R.E. (2004) Direct Numerical

Simulations of Plane Channel Flow over a 3D Cartesian Grid of Cubes. *The Proceedings of the 2nd International Conference on Porous Media and Applications*, Evora, 24-27 May 2004.

[24] Breugem, W., Boersma, B.J. and Uittenbogaard, R.E. (2005) The Laminar Boundary Layer over a Permeable Wall. *Transport in Porous Media*, **59**, 267-300. https://doi.org/10.1007/s11242-004-2557-1

[25] Kuznetsov, A.V. (1997) Influence of the Stress Jump Condition at the Porous-Medium/Clear-Fluid Interface on a Flow at a Porous Wall. *International Communications in Heat and Mass Transfer*, **24**, 401-410. https://doi.org/10.1016/S0735-1933(97)00025-0

[26] Kaviany, M. (1995) Principles of Heat Transfer in Porous Media. 2nd Edition, Springer, Berlin. https://doi.org/10.1007/978-1-4612-4254-3

[27] Whitaker, S. (1969) Advances in Theory of Fluid Motion in Porous Media. *Industrial and Engineering Chemistry*, **61**, 14-28. https://doi.org/10.1021/ie50720a004

[28] de Lemos, M.J.S. (2006) Turbulence in Porous Media.

[29] Pozrikidis, C. (2005) Effect of Membrane Thickness on the Slip and Drift Velocity in Parallel Shear Flow. *Journal of Fluids and Structures*, **20**, 177-187. https://doi.org/10.1016/j.jfluidstructs.2004.10.013

[30] Pozrikidis, C. (2004) Boundary Conditions for Shear Flow past a Permeable Interface Modeled as an Array of Cylinders. *Computers & Fluids*, **33**, 1-17. https://doi.org/10.1016/S0045-7930(03)00030-6

[31] Pozrikidis, C. (2010) Slip Velocity over a Perforated or Patchy Surface. *Journal of Fluid Mechanics*, **643**, 471-477. https://doi.org/10.1017/S0022112009992667

[32] Moureh, J., Tapsoba, M. and Flick, D. (2009) Airflow in a Slot-Ventilated Enclosure Partially Filled with Prousboxes: Part II—Measurements and Simulations within Porous Boxes. *Computer & Fluids*, **38**, 206-220. https://doi.org/10.1016/j.compfluid.2008.02.007

[33] Zong, C. and Zhang, G.Q. (2014) Numerical Modelling of Airflow and Gas Dispersion in the Pit Headspace via Slatted Floor: Comparison of Two Modelling Approaches. *Computers and Electronics in Agriculture*, **109**, 200-211. https://doi.org/10.1016/j.compag.2014.10.015

[34] Sun, H.W., *et al.* (2004) Development and Validation of 3-D Models to Simulate Airflow and Ammonia Distribution in a High-Rise™ Hog Building during Summer and Winter Conditions. *Agricultural Engineering International: The CIGR Journal of Scientific Research and Development*, **6**, 1-24.

[35] Bjerg, B., Zhang, B. and Kai, P. (2008) CFD Investigations of a Partly Pit Ventilation System as Method to Reduce Ammonia Emission from Pig Production Units. *The Eigth ASABE International Livestock Environment Symposium* (*ILES VIII*), Iguassu Falls, 1-5 September 2008.

[36] Dantec-Dynamics-SAS (2016) Système de Vélocimétrie Laser Doppler.

[37] Moureh, J. and Flick, D. (2005) Airflow Characteristics within a Slot-Ventilated Enclosure. *International Journal of Heat and Fluid Flow*, **26**, 12-24. https://doi.org/10.1016/j.ijheatfluidflow.2004.05.018

[38] Jin, Y. and Ogilvie, J.R. (1990) Near Floor Air Speeds from Center Slot Air Inlets in Swine Barns. ASAE Paper No. 90-4004, St-Joseph.

[39] Verhoff, A. (1963) The Two-Dimensional Turbulent Wall Jet with and without an External Stream. Rep. 626, Princeton University, Princeton.

[40] Rajaratnam, N. and Subramanya, K. (1967) Diffusion of Rectangular Wall Jets in

Wader Channels. *Journal of Hydraulic Research*, **5**, 281-294. https://doi.org/10.1080/00221686709500212

[41] Yu, H., Jou, L.-J., Ouyang, H.-T., *et al.* (2006) Similitude Criteria for a Two-Dimensional Wall Jet in an Isothermal Mechanically Ventilated Enclosure. *Biosystems Engineering*, **93**, 415-425. https://doi.org/10.1016/j.biosystemseng.2006.01.001

[42] Yu, H., *et al.* (2007) Scale Model Study of Airflow Performance in a Ceiling Slot-Ventilated Enclosure: Non-Isothermal Condition. *Building and Environment*, **42**, 1142-1150.

[43] Schälin, A. and Nielsen, P.V. (2004) Impact of Turbulence Anisotropy near Walls in Room Airflow. *Indoor Air*, **14**, 159-168. https://doi.org/10.1111/j.1600-0668.2004.00201e.x

[44] Schlichting, H. (1979) Boundary-Layer Theory.

[45] Kuwata, Y. and Suga, K. (2019) Extensive Investigation of the Influence of Wall Permeability on Turbulence. *International Journal of Heat and Fluid Flow*, **80**, Article ID: 108465. https://doi.org/10.1016/j.ijheatfluidflow.2019.108465

[46] Kong, F. and Schetz, J. (1982) Turbulent Boundary Layer over Porous Surfaces with Different Surface Geometries. *AIAA*, 20*th Aerospace Sciences Meeting*, Orlando, 11-14 January 1982. https://doi.org/10.2514/6.1982-30

[47] Manes, C., *et al.* (2009) Turbulence Structure of Open Channel Flows over Permeable And Impermeable Beds: A Comparative Study. *Physics of Fluids*, **21**, Article ID: 125109. https://doi.org/10.1063/1.3276292

[48] Silva, R.A. and de Lemos, M.J.S. (2003) Turbulent Flow in a Channel Occupied by a Porous Layer Considering the Stress Jump at the Interface. *International Journal of Heat and Mass Transfer*, **46**, 5113-5121. https://doi.org/10.1016/S0017-9310(03)00368-5

[49] Cannon, J.N., *et al.* (1979) A Study of Transpiration from Porous Flat Plates Simulating Plant Leaves. *International Journal of Heat and Mass Transfer*, **22**, 469-483. https://doi.org/10.1016/0017-9310(79)90013-9

[50] Naot, D. and Kreith, F. (1979) On the Penetration of Turbulence through Perforated Flat Plates. *International Journal of Heat and Mass Transfer*, **23**, 566-568. https://doi.org/10.1016/0017-9310(80)90099-X